Understanding the evolution of organic fouling in membrane distillation through driving force and resistance analysis

Understanding the evolution of organic fouling in membrane distillation through driving force and resistance analysis

[1] Department of Environment, Land and Infrastructure Engineering (DIATI), Politecnico di Torino, Corso Duca degli Abruzzi 24, Turin, 10129, Italy

[2] CleanWaterCenter@PoliTo, Corso Duca degli Abruzzi 24, Turin, 10129, Italy

[3] Water Desalination and Reuse Center (WDRC), Biological & Environmental Science & Engineering Division (BESE), King Abdullah University of Science and Technology (KAUST), Thuwal 23955-6900, Saudi Arabia

Highlights

- Flux decline and fouling thickness are linearly correlated.
- The feed to permeate heat transfer decreases during fouling.
- OCT allows direct analysis of the fouling layer development.
- Fouling thickness is governed by the permeate drag force and shear stress increment.
- The balance between driving force and resistance yields a stationary flux.

Abstract

Fouling is one of the main issues hampering the implementation of thermally-driven membrane distillation (MD). While the mutual influence of driving force and fouling deposition has been critically assessed in pressure- and osmotically-driven processes, fouling mechanisms have not been fully understood in MD. Using non-invasive optical coherence tomography, this study describes for the first time the evolution of resistance and driving force evolution during the development of the organic fouling layer in direct contact MD. Foulant layer thickness was found to be strongly and linearly correlated to water flux under different conditions of feed temperature and cross-flow velocity. Experimental and modeling results indicate that this phenomenon is associated to the increase of the overall resistance to water vapor transport. With a clean membrane, heat loss is mainly governed by the permeate flux and by temperature polarization. As fouling evolves over time, temperature polarization increases and affects, together with the additional fouling resistance, the water flux and the heat transfer from feed to permeate. Indeed, foulant accumulation was observed to lead to a gradual reduction of heat transfer from the feed to the permeate side, causing a steady increase of the average nominal driving force, i.e., difference between vapor tension in the feed bulk and in the permeate bulk. The driving force and the resistance evolved together during this dynamic process of fouling development, resulting in the achievement of a near-stable flux value over time.

Keywords: membrane distillation; optical coherence tomography (OCT); organic fouling; fouling evolution; driving force.

1 Introduction

Membrane distillation (MD) is a thermally-driven process for water desalination and for the concentration of challenging wastewater and hypersaline feed [1]. The simplest of the MD configurations is the so-called direct contact membrane distillation (DCMD). In DCMD, the warmer feed solution is separated from the colder distillate product by a semi-permeable hydrophobic membrane that only allows, under ideal conditions, the passage of water vapor [2]. The driving force is linked to the temperature difference between the warmer feed solution and the colder distillate stream. MD has been mainly investigated for desalination purposes, but recent interest has grown also for the treatment of produced waters, surface waters, and groundwaters with the goals of reuse and/or stream concentration [3-7]. These feed solutions are all characterized by the presence of organic substances, often consisting of natural organic matter and humic acids (HA). Srisurichan *et al.* showed that when HA is combined with $CaCl_2$, a heavy and dense HA foulant layer forms during MD operation and results in a significant flux decline and increase of the heat transfer resistance [8].

It is generally accepted that organic fouling in pressure-driven membrane processes is more severe than in MD [9, 10]. On the other hand, fouling in MD is also still believed to be one of the main factors limiting the commercial use of this technology [11]. In direct contact membrane distillation, fouling involves both mass and heat transfer, which are highly interconnected with each other. Here, fouling formation on the membrane surface affects the mass transfer across the membrane, causing a decline in permeate flux. Since the permeate flux is also responsible for transferring latent heat of vaporization from the feed to the permeate side, as fouling evolves, also the heat flow decreases. In particular, the overall heat transfer decreases during fouling in MD both due to the permeate flux decline and for the formation of an additional thermally insulating layer [12]. Moreover, the fouling

layer results in temperature polarization, causing large temperature deviations with respect to the nominal gradient [13]. In this complex phenomenon, the degree of resistance can be theoretically calculated based on the characteristics of the fouling layer, such as its thickness and porosity [8, 14]. However, the available data are usually not sufficiently accurate as the fouling layer has been mainly characterized by destructive techniques, limiting the possibility of providing insight into its development over time [15]. Indeed, so far, most studies on fouling in MD have limited their scope to the water vapor productivity along the filtration time or the recovery rate value [16, 17]. In recent years, optical coherence tomography (OCT) has been used to conduct non-invasive dynamic analysis of the fouling development in membrane systems [18, 19]. OCT allows spatial and time monitoring of fouling development on the membrane module with micron resolution, as well as morphological investigation of the deposited layer [20].

For the first time in this study, the OCT technology is used in combination with continuous flux and temperature measurements to provide a complete assessment of fouling behavior in direct contact membrane distillation and to identify the main factors dominating mass and thermal transfer during this process. For this purpose, a feed with high load of humic acids is used as of particular interest for MD applications and also due to the homogeneous deposition that this matrix is able to form on the membrane surface, allowing more reliable data analysis through the OCT. Moreover, the contributions of the various resistances to mass transport are simultaneously analyzed and correlated to the loss of water vapor productivity. As in the osmotic and pressure driven membrane processes, fouling thickness evolution and the overall fouling behavior are linked to the variation of the driving force and the fouling resistance. The permeate drag force and the shear stress also increase during distillation showing a counteracting effect on the foulant deposition. Finally, important insight into the fouling mechanism in MD under a wide range of realistic operating

conditions is provided and a new mechanism relating fouling to the magnitude of driving force and resistance in DCMD is discussed.

2 Materials and Methods

2.1 Membrane characteristics and feed solution composition.

A synthetic feed solution with an initial humic acid (HA, Sigma-Aldrich) concentration of 500 mg/L was employed in this study. To accelerate the fouling deposition and to enhance high load of HA solubilization, 20 mM of calcium chloride ($CaCl_2$, Sigma-Aldrich) was also added to the feed solution [8, 25]. These concentrations of organics and salts can be typical of produced water streams [17], for which MD is particularly appealing, but it is important to note that a high load were mainly selected to accelerate fouling and to simulate an overall mass flow of foulants that can be observed under long term operation in up-scaled systems. Initial volumes of 1 L were used for both the feed and the distillate solutions. For the feed, 500 mL of pure water were initially used for each test to evaluate a stable initial water flux. After stabilization, a stock solution was added to reach the desired feed volume and concentrations. The concentrate stock addition indicates the beginning of the fouling test. For all the experiments, a commercially available membrane consisting of a hydrophobic polytetrafluoroethylene active layer with a polypropylene support (PP-PTFE) (Membrane Solutions corp., US) was used. The membrane characteristics are listed in Table 1, with several data provided by the manufacturer. The membrane permeability coefficient was experimentally determined by measuring the water flux and dividing it by the calculated vapor pressure difference across the membrane at the operating temperatures.

Table 1. Porous PP-PTFE membrane characteristics

Parameter	Value	Units	Source
Thickness	174 - 245	µm	manufacturer
Mean pore size	0.22	µm	manufacturer
Bubble point	16-20.3	psi	manufacturer

Permeability coefficient	144	kg m^{-2} $h^{-1}$$bar^{-1}$	experiments

2.2 Direct contact membrane distillation lab system

All the MD tests were performed in direct contact membrane distillation (DCMD) configuration with a lab-scale flow-cell where the warm feed and the cold permeate were flowed in countercurrent mode. The warm liquid stream is in direct contact with the membrane, which allows vapors to pass and then condense at the distillate side in the cold water stream that is also in contact with the membrane. The DCMD flow-cell was made of polymethyl methacrylate and customized to allow in-situ characterization with OCT (see section 2.4). The flow-cell had an active membrane area of 33 cm^2 with dimensions of 10 × 3.3 cm (length × width). Flow-cell images are reported in Fig S1 of the Supporting Information file (SI) together with the overall setup describe here below. The temperatures in the warm feed and cold permeate inlet streams were maintained constant throughout each experiment using two separate heating circulators keeping the desired water temperature inside an insulated stainless-steel bath(Corio-CD, Julabo, Germany), in which the coil circulating the streams was immersed. The temperature sensors were integrated in the conductivity meters (TetraCon 325, Xylem Analytics, Germany) located just before the inlet of the flow-cell. Before foulant addition, those sensors allowed measurements of the stream temperatures entering the flow-cell and the right settings of the heating circulators to get the desired inlet temperature of the two streams. Two more sensors were used to measure the outlet temperature values of the feed and the permeate streams during operation. Cross-flow velocities of both water streams were measured by digital flow meters (MINI CORI-FLOW^{TM}, Bronkhorst, Netherlands). The flux across the membrane was calculated from the change in weight of the permeate tank over time, measured through a computer-interfaced balance. All the instruments were digitally connected and controlled by Lab View software (National Instruments, United States).

2.3 Operating conditions and protocol of the fouling experiments

In this study, we investigated feed temperatures in the range of 35 - 65 °C and feed cross-flow velocities in the range of 0.2 - 0.4 m/s. Constant temperature of 20 °C and cross-flow velocity of 0.1 m/s were maintained on the permeate side. The central composite design method was used in Design Expert software to identify an efficient set of experiments within the ranges of the selected feed temperatures and flow velocities (see Table S1, SI). For all the experiments, the flux was first stabilized using de-ionized water as feed solution, without organic foulants, thus obtaining a steady-state flux value referred to as J_{w0}. The fouling phase started when an appropriate volume of organic foulant stock solution was added into the feed tank and it was run until a volume concentration factor of 2.5 was achieved. A schematic presentation of the described protocol is showed in Fig. S2. The decrement of flux (J_w) observed during the fouling phase can be largely attributed to foulant deposition as salinity in the feed solution was low. The maximum reduction of the feed vapor tension during tests was 0.02% from the initial value due to $CaCl_2$ concentration (reduction due to HA concentration was even more negligible, since HA accounted for less than 20% of the total contaminants weight). Therefore, the flux decline ratio (J_w/J_{w0}) decreased during operation due to fouling. This parameter was adopted to allow an easier correlation between flux and the fouling layer thickness analyzed through the OCT, which is described in the next section.

2.4 Direct monitoring of the fouling thickness with OCT

A spectral-domain optical coherence tomography (SD-OCT) system (Ganymede II, Thorlabs GmbH, Germany) was used to assess the fouling deposition on the membrane surface. The instrument was equipped with a scan lens (LSM 03BB). The OCT probe was positioned on top of the middle point along the length of the DCMD flow-cell, to monitor the fouling layer development over time. Two-dimensional cross-section OCT scans were taken over a transversal area of 8.0 × 2.6 mm^2 (length × depth). FiJi software was used to process the OCT

images by reducing the noise and adjusting contrast and brightness. The fouling layer thickness was calculated from the OCT images using a custom-made MATLAB code.

2.5 Heat transfer analysis

Heat balances

The heat balances over permeate volume (eq. (1)) and over the whole flow-cell (eq. (2)) can be written in terms of heat flows (or power), Q (J/s), here with incoming heat streams on the left-hand side and outgoing on the right-hand side of the balance equations:

$$F_{P,in}\rho C_P T_{P,in} + Q_M = \left(F_{P,in} + F_w\right)\rho C_P T_{P,out} + Q_{P,loss} \quad (1)$$

$$F_{F,in}\rho C_P T_{F,in} + F_{P,in}\rho C_P T_{P,in} = \left(F_{F,in} - F_w\right)\rho C_P T_{F,out} + \left(F_{P,in} + F_w\right)\rho C_P T_{P,out} + Q_{F,loss} + Q_{P,loss} \quad (2)$$

F_F and F_P are the volumetric flow rates (m^3/s) on the feed and permeate side of the membrane; T_F and T_P are the bulk temperatures (K) of feed and permeate, all at inlet and outlet (denoted by indices *in* and *out*). It is assumed that the heat capacity of water is approximately constant between 20 and 60 °C, with C_P = 4180 J $kg^{-1}K^{-1}$, and the water density can also be taken as constant, ρ = 998 kg/m^{-3}. The heat balances can be further simplified by assuming that the total flowrate of water passing the membrane, F_w, is negligibly small compared with the flows of feed and permeate ($F_w << F_{P,in}, F_{F,in}$). Also, the heat loss from the permeate side to exterior, $Q_{P,loss}$, can be neglected because the permeate temperature is very close to the ambient temperature, thus heat losses predominately occur at the hot side of the system as $Q_{F,loss}$. By introducing the notations for heat flows between inlet and outlet, Q_P for permeate side and Q_F for feed side:

$$Q_P = F_P \rho c_P \left(T_{P,out} - T_{P,in}\right) \quad (3)$$

$$Q_F = F_F \rho c_P \left(T_{F,in} - T_{F,out}\right) \quad (4)$$

194 the heat balances over permeate (eq. (5)) and over the flow-cell (eq. (6)) become:

195 $$Q_M = Q_P \quad (5)$$

196 $$Q_{F,loss} = Q_F - Q_P \quad (6)$$

197 Eq. (5) means that the permeate heat gain, Q_P, is a result of the total heat transfer through the
198 membrane $Q_M = Q_w + Q_m$ caused by the condensation of water, Q_w, and by conduction, Q_m.
199 Eq. (6) allows the estimation of heat loss through the feed channel walls to the exterior, as the
200 difference between the power change between inlet and outlet for feed and permeate.

201 *Temperature drop from feed to permeate*

202 In DCMD, heat is transferred from the feed to the permeate side by several mechanisms. First,
203 there is conduction from the warmer feed solution (bulk temperature T_F) across a thermal
204 boundary layer to the surface of the fouling layer (temperature $T_{F,L}$), which links to the
205 temperature polarization on the feed side. Second, if there is a fouling layer, this will induce an
206 additional heat transfer resistance by conduction, usually named cake-enhanced temperature
207 polarization, with a temperature drop from $T_{F,L}$ to $T_{F,M}$ at the membrane surface. Third, several
208 heat transfer mechanisms take place in the membrane: conduction through the membrane
209 polymeric material, conduction through the vapors in the pores (which may be negligible), and
210 an important heat flux due to evaporation/condensation at the feed/permeate interfaces. Finally,
211 there is also temperature polarization on the permeate side, with conduction in the quasi-
212 stagnant water layer adjacent to the membrane driven by the difference between $T_{P,M}$ at the
213 membrane surface at T_P in the bulk permeate.

214 The average temperature value in the feed and permeate side, T_F and T_P, was the arithmetic
215 mean of measured inlet and outlet water temperatures. The difference between the feed and

permeate bulk temperature give the total temperature drop between the feed and permeate across the thermal boundary layers ($\Delta T_F, \Delta T_P$), foulant layer (ΔT_L) and membrane (ΔT_M):

$$T_F - T_P = \Delta T_F + \Delta T_L + \Delta T_M + \Delta T_P \quad (7)$$

However, the individual temperature differences can also be estimated. Assuming the existence of a fouling layer, the continuity of total heat flux through the membrane, q_M (J m^{-2}s^{-1}), implies:

$$q_M = h_F\left(T_F - T_{F,L}\right) = h_L\left(T_{F,L} - T_{F,M}\right) = h_M\left(T_{F,M} - T_{P,M}\right) = h_P\left(T_{P,M} - T_P\right) \quad (8)$$

with the four heat transfer coefficients (J m^{-2}s^{-1}K^{-1}) as h_F and h_P for thermal boundary layers on the feed and permeate side, h_L through the fouling layer, and h_M though the membrane (a lumped value involving both evaporation/condensation and conduction). With the heat flux as heat flow $Q_M = Q_P$ divided by membrane area, A_M (0.0033 m^2), one can express the temperature differences across the different layers:

$$\Delta T_F = T_F - T_{F,L} = \frac{Q_P}{h_F A_M}, \qquad \Delta T_L = T_{F,L} - T_{F,M} = \frac{Q_P}{h_L A_M}$$

$$\Delta T_M = T_{F,M} - T_{P,M} = \frac{Q_P}{h_M A_M}, \qquad \Delta T_P = T_{P,M} - T_P = \frac{Q_P}{h_P A_M}$$

Average heat transfer coefficients through the thermal boundary layers, h_F and h_P, may be estimated from correlations for the Nusselt number, $\mathrm{Nu} = hH/k$, function of Reynolds number, $\mathrm{Re} = uH\rho/\mu$, and Prandtl number, $\mathrm{Pr} = C_p\,\mu/k$. These involve the physical properties of water (density ρ, dynamic viscosity μ, specific heat C_p and thermal conductivity k), as well as the water velocity u and the height H of the specific channel (feed or permeate) that decreases at the feed side in time due to the growth of the fouling layer. While ρ, C_p and k (0.6 J s^{-1}m^{-1}K^{-1}) can be assumed constant in the interval of temperatures, viscosity has a significant change taken as $\mu = 0.497\left(42.5 + T\right)^{-1.5}$ with T in °C. Generally, convective heat

transfer correlations are developed based on the assumption of small rate of mass transfer. We adopted the Nusselt relation for heat transfer between two plates, for both feed and permeate channels, $\mathrm{Nu} = 0.664\,\mathrm{Re}^{1/2}\,\mathrm{Pr}^{1/3}$. This allows estimation of $\Delta T_F = \frac{Q_P}{A_M}\frac{H_F}{k_F \mathrm{Nu}_F}$ and $\Delta T_P = \frac{Q_P}{A_M}\frac{H_P}{k_P \mathrm{Nu}_P}$. The fitting of experiments before foulant addition also allowed a determination of the temperature difference across the membrane as a function of the measured flux (see Fig. S3), $\Delta T_M = f\left(J_w\right)$, where the water flux is $J_w = F_w / A_M$. Finally, the temperature drop over the fouling layer can be computed during each test by:

$$\Delta T_L = T_F - T_P - \Delta T_F - \Delta T_M - \Delta T_P = \frac{Q_P}{A_M}\frac{\delta_L}{k_L}$$

This assumes heat transfer through the fouling layer occurs predominately by conduction.

Equations were implemented in custom MATLAB code processing OCT and MD data acquired during each test. The value of k_L was thus retrieved for each test prior assuming this value as 0.6 W $m^{-1}K^{-1}$, i.e., water thermal conductivity. Thus, this value was assumed constant to retrieve the Nusselt number during fouling evolution for each test.

2.6 Driving force and fouling resistance analysis

In MD, the driving force for the mass transfer is provided by the water vapor pressure difference between the feed, p_F, and the permeate side, p_P. The vapor pressure p (Pa) for water can be calculated from the Antoine equation $p = \exp\left(23.238 - 3841/\left(T - 45\right)\right)$ with T in K. The nominal driving force calculated in this study is based on the average value from the inlet and outlet bulk temperatures of the feed stream, T_F, and the permeate stream, T_P. The overall resistance to mass transfer between feed and permeate, R, was calculated as ratio between the driving force DF and the measured water vapor flux J_w [24]:

$$R = \frac{DF}{J_w} = \frac{p_F - p_P}{J_w} \quad (9)$$

Changes in the driving force and in the resistance were evaluated during the tests to determine the mechanism of fouling development.

3 Results and discussion

3.1 Impact of temperature and cross-flow velocity on process performance and fouling development

Fouling evolution in membrane distillation was evaluated in this study under different realistic conditions of feed inlet temperature ($T_{F,in}$) and cross-flow velocity (u_F). As expected, the initial flux was strongly correlated to the applied feed inlet temperature. Results reported in Fig. S4 suggest that the initial flux can be increased from ~3 to 22.5 kg $m^{-2}h^{-1}$ by increasing $T_{F,in}$ from 35 to 65 °C. This is a result of the nature of the MD driving force, i.e., the vapor tension difference between the feed and the permeate [26]. On the other hand, an almost negligible effect on J_w was observed when increasing the cross-flow velocity. Indeed, despite u_F plays a role on the heat transfer coefficient and consequent temperature polarization, this effect was negligible compared to the applied feed temperature. It is also important to note that in this study the membrane housing length was sufficiently small to minimize the temperature profiles along the cross-flow direction.

The fouling layer development over time was monitored with OCT microscopy. Fig. 1 presents representative OCT scans obtained for tests performed with applied feed inlet temperatures of 35, 50, and 65 °C, and acquired at the three volume concentration factors (VCF) of 1.3, 1.8, and 2.5. Images refer to the tests performed at a cross-flow velocity of 0.3 m/s. The fouling layer always increased during distillation: in details, the measured thickness when operating at

65 °C and 50 °C changed from 622 µm to 1013 µm and from 355 µm to 878 µm, respectively, when the VCF was increased from 1.3 to 2.2. Indeed, for all VCF values reported in Fig 1, a decrease of fouling layer thickness was observed when the feed inlet temperature was lowered. Interestingly, considerable lower deposition was observed for the experiment performed at 35 °C, whereby thickness only changed from 196 µm to 273 µm in the same VCF range. Therefore, the fouling deposition rate in DCMD may be directly linked to the feed temperature: severe organic fouling is observed at higher temperatures.

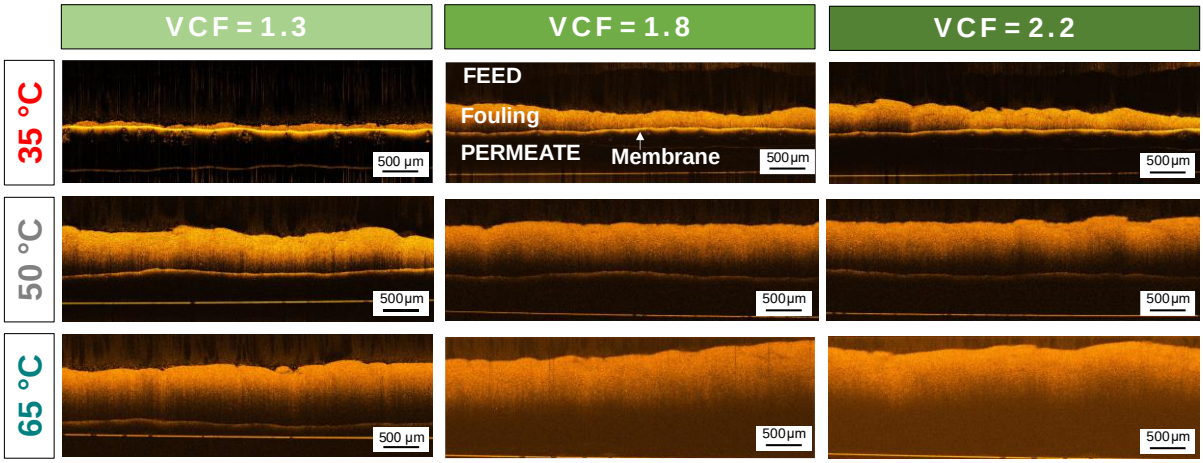

Fig. 1. Cross-sectional OCT scans of the fouling layer deposited on the membrane surface, at three VCF values, for experiments performed at fixed cross-flow velocity of 0.3 m/s and with different inlet feed temperatures (35, 50, 65 °C). The OCT scans were acquired at the middle position of the membrane cell during continuous operation.

The dependency of flux decline ratio and fouling thickness on the VCF is shown in Fig. 2. In general, the flux decline (Fig. 2a1) showed a similar behavior of fouling layer thickness (Fig. 2a2). This evidence highlights how these parameters are similarly influenced by the different applied conditions of $T_{F,in}$ and u_F. The cross-flow velocity mainly influenced the flux and fouling deposition at lower inlet feed temperatures: the J_w/J_{w0} varied from 0.8 to 0.6 (higher flux decline) when decreasing u_F from 0.40 to 0.25 m/s at 40 °C, while negligible influence on the final value of J_w/J_{w0} was observed by changing the u_F for the experiments performed at 50 and 60 °C. Symmetrically, lower final layer thickness was observed when increasing the cross-

flow velocity at 40 °C, from 538 µm to 313 µm, while negligible difference was obtained when the u_F was increased at a $T_{F,in}$ of 50 °C and 60 °C. This effect could be attributed to the reduced ability of the cross-flow velocity in counteracting fouling when operating at higher flux. On the other hand, a strong effect was played by $T_{F,in}$, whose increase generally reduced the value of J_w/J_{w0} and evidently increased the fouling deposition along the VCF. This result is in good agreement with previous studies and may be correlated to the role of temperature in increasing both initial flux (see Fig. S4) and temperature polarization [27-29].

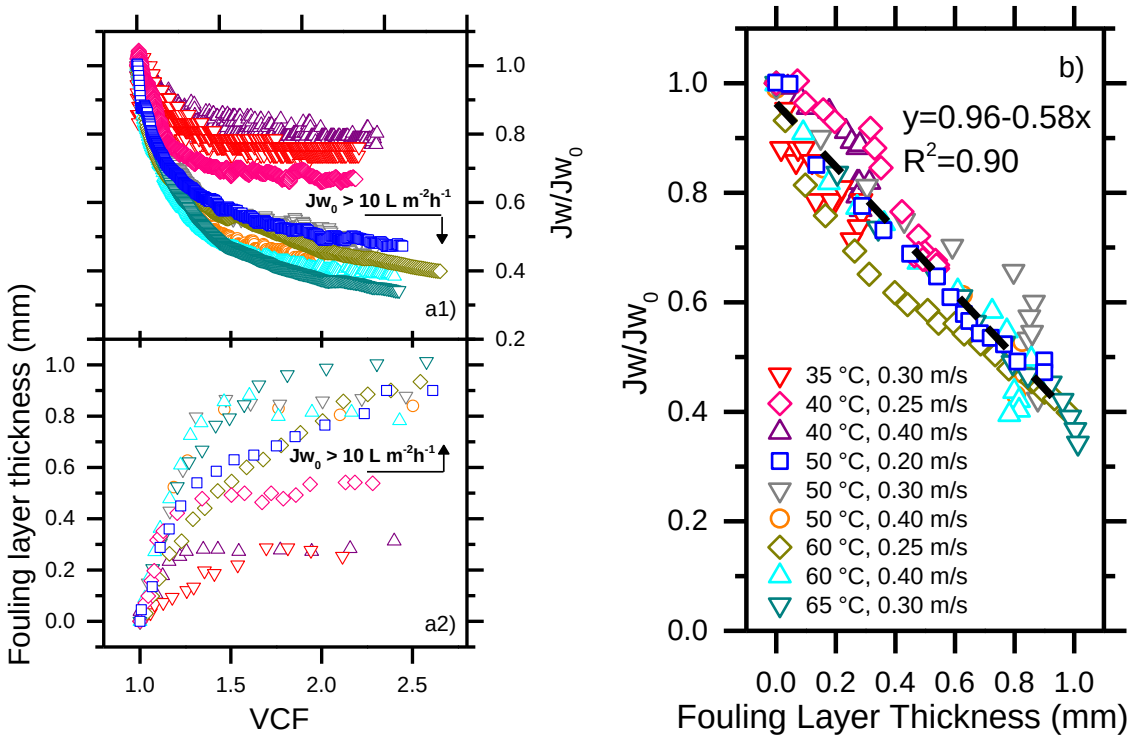

Fig. 2. (a1) Normalized flux J_w/J_{w0} and (a2) fouling thickness development plotted against VCF. The experiments were performed with the synthetic feed water in the presence of humic acid and calcium at different initial permeate flux J_{w0} obtained by varying the feed inlet temperature $T_{F,in}$ and the cross-flow velocity u_F in DCMD configuration. Fouling layer thickness was determined from the OCT scans acquired in the middle position of the cell during continuous operation. (b) The correlation between fouling layer thickness and normalized permeate flux. The coefficient of determination R^2 is for the line fitting all the experimental data.

Interestingly, from the data presented in both Fig. 2a1 and 2a2, it is possible to notice the presence of a low- and a high- fouling region, respectively, below and above the initial flux of

roughly 10 L $m^{-2}h^{-1}$. Note that J_{w0} below this value are obtained when experiments are performed at a feed temperature below 50 °C (see Fig. S4), confirming previous findings [7, 19, 25]. In parallel, below this $T_{F,in}$ value, also considerable lower foulant accumulation was measured (see Fig. 2a1). Previous studies linked the presence of different fouling regions to the existence of a possible threshold flux [30]. The concept of critical or threshold flux has been widely reported in osmotically-and pressure-driven membrane processes [22, 31].

Fig. 2b shows the flux decline J_w/J_{w0} as a function of the fouling layer thickness, both measured at different times during the various experiments. Overall, the data reflect the inverse linear dependency between the two parameters, regardless of the experimental conditions (R^2=0.9 for the aggregate regression). This result is in agreement with previous studies on wastewater treatment with MD and confirms how, as in the other membrane separation process, the flux decline during long-term operation is directly correlated to the amount of fouling deposited on the membrane surface [32, 33]. A possible explanation of this strong correlation is associated with the magnitude of the driving force for water separation (vapor tension difference between feed and permeate side of the membrane). Any loss of flux may be caused by a corresponding percentage of the driving force lost along the fouling layer thickness, a phenomenon named cake-enhanced temperature polarization [28, 29, 34]. Such simple linear correlation implies the possibility to obtaining a reasonable estimation of the foulant accumulation based on flux data during DCMD operation for a wide range of feed inlet temperatures and cross-flow velocities. From this prospective, there is still a lack of knowledge related to modelling of foulant deposition in DCMD.

In summary, this investigation highlights how flux decline rate and fouling layer thickness similarly increased with the feed temperature and closely correlated with initial flux. On the other hand, the value of the cross-flow velocity did not show a clear influence on flux, while it mainly decreased the fouling layer thickness. Interestingly, a low fouling region was identified

when operating below 50°C of inlet feed temperature. Finally, strong linear correlation between the fouling layer development and the vapor permeate flux was observed.

3.2 Analysis of the factors contributing to the temperature evolution during fouling

The membrane, the fouling layer, and temperature polarization layers can be seen as a series of resistances to water flux, as each layer accounts for a certain amount of heat loss from the hot to the cold side. Thus, the nominal driving force (vapor tension difference between bulk feed and permeate) is lowered to a net driving force across the membrane (vapor tension difference between the two membrane interfaces, at the feed and at the permeate side). The temperature profile on both the feed and the permeate side before foulant addition (clean membrane) was retrieved for all the experiments from Eq.7, which also accounts for temperature polarization. The temperature drop across the membrane was then retrieved as a difference between the temperature values as a result of polarization in the two channels. Linear interpolation of these results, shown in Figure S3, allowed estimation of the temperature drop across the membrane for any flux values observed during the experiments. The growth of a fouling layer exacerbated the driving force losses, which added to the effects already present for clean membranes.

The separate contribution of each heat transfer resistance from feed to permeate during the fouling process is presented in Fig.3. The temperature profile was plotted against the fouling layer thickness and calculated by Eqs. 1-7. In all tests, the temperature loss due to polarization decreased during fouling (see blue color bands in Fig 3), due to the decrement of the heat flow from feed to permeate (Eq. 3). This is due to the increment of the total heat subtracted by the increasing fouling thickness fouling and by the decrement of permeation (see orange and green color bar in Fig 3, respectively). According to the model, the feed temperature polarization (ΔT_F) reduction was more pronounced than that in the permeate

stream (ΔT_P), because the fouling layer growth also decreased the effective height of the feed channel. This effect can be observed under all the tested conditions in Fig 3, by comparing the two blue bands with each other. The foulant layer thickness influences the feed temperature polarization term, due to the heat flow reduction from feed to permeate and also because the reduction of flow channel height increases the cross-flow velocity, which thereby decreases the temperature boundary layer thickness. On the other hand, an enhanced cross-flow velocity leads to more shear stress over the fouling layer, which can be accountable for the decreasing effective deposition of foulants in time. This mechanism can explain the gradual approach of a foulant thickness plateau during the last phase of the experiments (see Fig. 2a2).

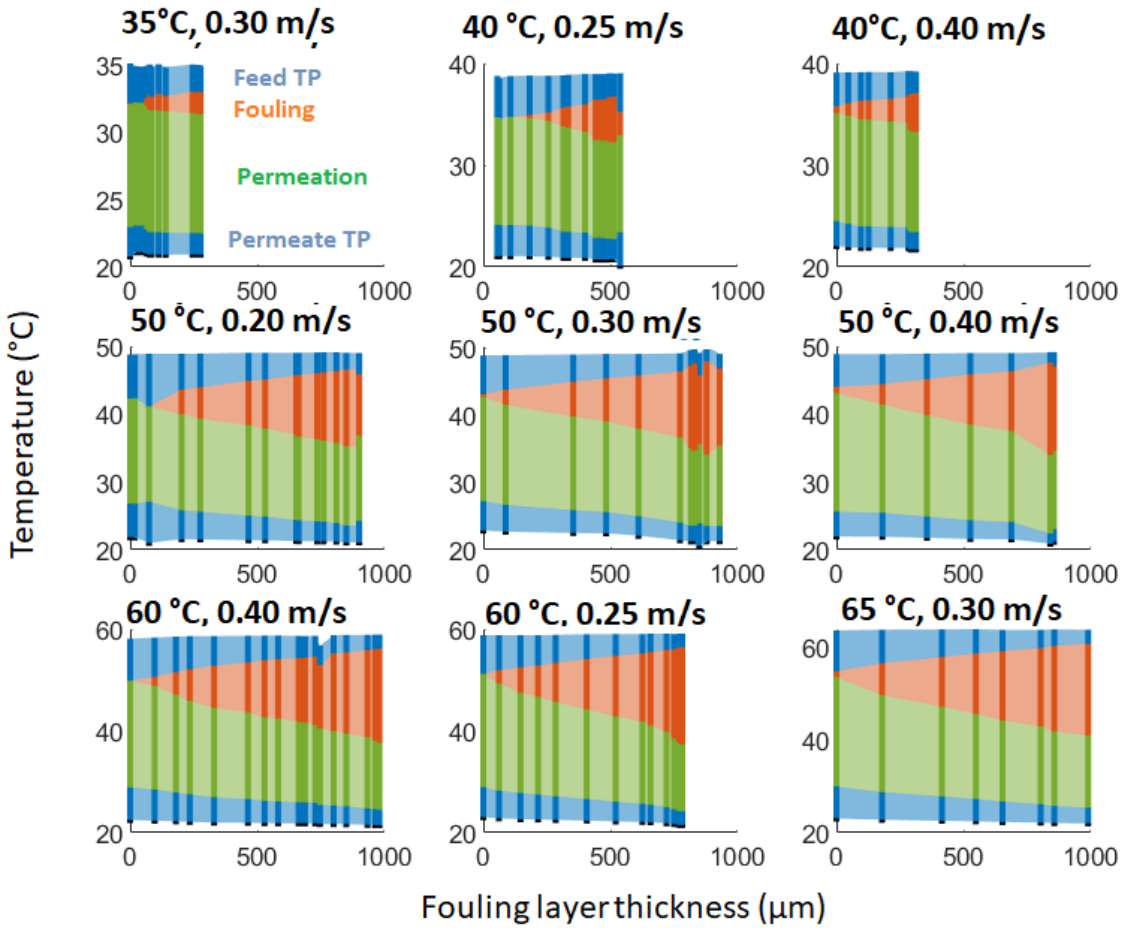

Fig. 3. Separate contributions of each heat transfer resistance in the overall temperature loss, estimated during fouling development for experiments performed in different conditions. The

uppermost and lowermost values indicate the bulk temperatures in the feed and permeate during fouling, as average between the measured inlet and outlet temperature. Blue areas: temperature polarization in feed (ΔT_F, top) and permeate (ΔT_P, bottom); Red area: temperature drop through fouling layer (ΔT_L); Green area: temperature drop over the membrane (water vapor flux contribution, ΔT_M).

In all tests, the water vapor heat flow generally decreased as fouling accumulation occurred (see green band in Fig. 3). Indeed, higher feed temperatures generate more rapid flux decline, which is here reflected by the higher discrepancy in the amount of heat loss due to permeation from the beginning to the end of the tests when increasing the feed inlet temperature. As an example, the test at 35 °C shows a heat loss due to permeation of roughly 10 °C during the entire duration of the test, while at 65°C feed bulk temperature, the related heat loss decreased from 30°C to 20 °C throughout the test. In parallel, the analysis allows estimation of the amount of heat subtracted by the growing fouling layer. This portion gradually increased in all the experiments as fouling layer thickness evolved as a result of foulant deposition, while both temperature polarizations and convective heat decreased. Once again, as the fouling thickness is mainly governed by the feed temperature, heat subtracted by the fouling layer increased more for tests performed at higher temperatures. As an example, the highest difference can be observed by comparing again the 35 °C and 65 °C test, where the final temperature decline within the fouling thickness was about 3 °C and 20 °C, respectively. In other words, while the loss of driving force is related mainly to temperature polarizations and water vapor flux with a clean membrane, fouling becomes relatively more and more significant in terms of driving force losses compared to the other two phenomena during operation. Interestingly, this behavior evolved similarly regardless of the operational conditions.

Another consideration resulting from the analysis is that a small variation of the two average bulk temperature profiles from initial values occurred during operation. Specifically, the

409 average bulk feed temperature was estimated to increase while the average permeate
410 temperature to decrease slightly as organic foulants deposited onto the membranes. This
411 mechanism translated into an overall small increment of the nominal (bulk) driving force, the
412 net effect of a gradually lower amount of heat transferred from the feed to the permeate side
413 due fouling accumulation and the concomitant flux decline. In other words, the average
414 nominal driving force in the membrane housing increased in time, while the net driving force
415 decreased due to foulant accumulation. Despite the effect on the bulk driving force was not
416 particularly pronounced in this study due to the small size of the membrane, it has important
417 implications on the fouling evolution, discussed in depth below, and it would be much more
418 significant in large-scale systems.

419 **3.3 Overall driving force and resistance analysis during fouling in DCMD**

420 To approach a mechanistic explanation of how fouling evolves in DCMD, the driving force
421 (*DF*) and the fouling resistance (*R*) are investigated in this section in the light of the measured
422 fouling layer thickness. Fig. 4 shows the values of the two parameters calculated for
423 experiments performed under different conditions of feed inlet temperature and cross-flow
424 velocity. A linear fit was calculated for each experiment, with intercept and standard error
425 values reported in Table S2 (SI). The overall resistance to the permeate flux was calculated by
426 Eq. 8. All tests started with similar resistance in the range between 700 and1000 Pa m^2 h kg^{-1},
427 as highlighted by the intercept values in Figure 4a. Results imply that fouling deposition
428 inevitably leads to the development of an additional resistance: the good quality of the linear
429 fit implies the role of the fouling thickness on the proportional increment of total resistance,
430 consistent with the discussion of the sections above. Furthermore, the rate of resistance
431 increment was dependent on the operating conditions, possibly due to the different flux decline
432 rates (Fig. 2).

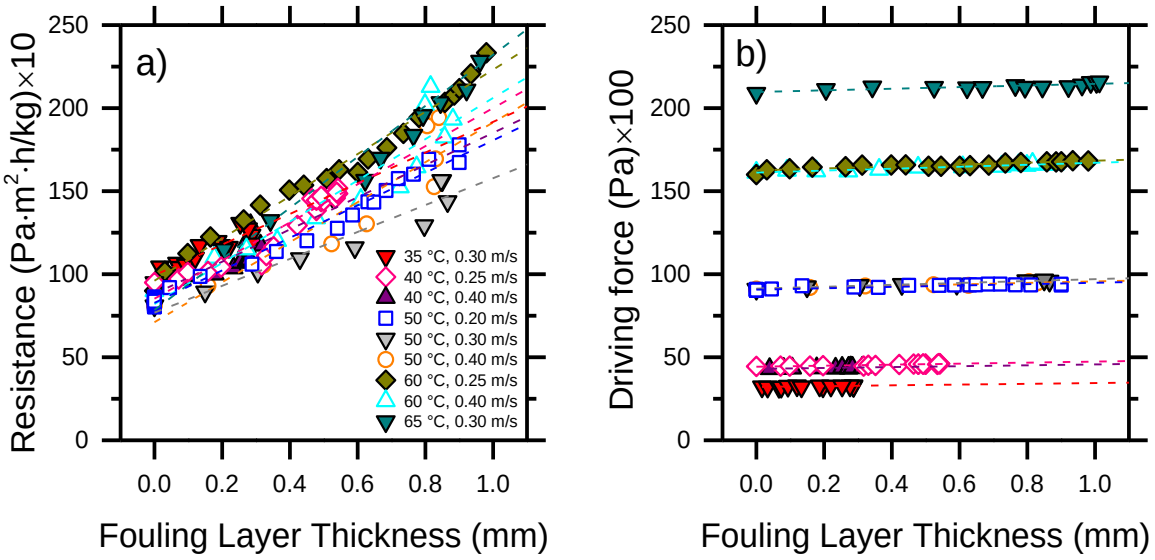

433 **Fig. 4.** (a) Total resistance, *R*, and (b) nominal driving force, *DF*, calculated from the data
434 reported in Fig. 1, as a function of the foulant thickness. The fits are shown by dash line with
435 the respective colors. The multiplicative factors indicates that the showed y-axes values must
436 be multiplied for ten and one hundred to get the real R and DF values, respectively.

437

438 The initial values of the total driving force depend solely on the initial operating feed
439 temperatures. As discussed in the previous section, organic fouling caused an increase in the
440 average nominal driving force, rationalized with the decrement of the heat transfer from the
441 feed to the permeate [35]. The slopes reported in Table S2 suggest that also this effect was
442 somewhat proportional to the initial temperature. In summary, both the total resistance and the
443 bulk driving force increased during operation. A clearer picture of this mutual increment can
444 be observed in Fig. S5, reporting results for all the experiments performed at 50 °C. It is
445 important to note that, while the reduction in polarization phenomena with fouling is present
446 in all membrane-based filtration processes, the increment of the nominal driving force during
447 fouling is not a mechanism shared by all filtration processes. For example, in pressure-driven
448 membrane processes, the nominal driving force is largely independent of foulant deposition, as
449 the fouling layer has not been found to significantly influence the pressure profiles within the
450 channels of the membrane housing or module [22, 24]. To summarize, during fouling
451 deposition both the total resistance and the average nominal driving force increased, translating

into a nearly constant net driving force, hence stabilized flux, attained after a certain time. This phenomenon is mainly attributed to a decrement of the convective heat flow from the feed to the permeate as an additional resistance is generated by fouling layer accumulation.

3.4 Proposed fouling evolution mechanism in DCMD

Although fouling is a continuous process, it can be also described as the result of discreet steps to mechanistically depict the evolution of deposition as governed by the mutual increment of the driving force and mass transfer resistance (Fig. 5). This type of mechanistic model has already been used in osmotically- and pressure-driven processes, since it is not dependent on the nature of the driving force [21]. According to the results obtained in this study, the increase of the fouling layer thickness on the membrane surface linearly increased the total resistance to the water vapor flux. This phenomenon was found to be analogous under a wide range of investigated conditions. The increase in resistance translated into a heat transfer reduction from the feed to the permeate side and a consequent increment of the average nominal driving force, i.e., the difference between the average bulk temperature of the feed and of the permeate stream. This increase in driving force and the reduction of polarization outside the fouling layer inevitably caused the permeate drag force to increase, likely causing more foulant deposition. The feedback between driving force and resistance continued to evolve as fouling thickness increased in a framework whereby also hydrodynamic conditions were influenced by the growing layer. In the schematic of Fig. 5, it can be observed how in the initial stage of fouling, the permeate drag should dominate fouling deposition as only partially counterbalanced by the shear stress. A strong decrement of the permeate flux is observed as result of fouling accumulation (Fig. 5a). However, with layer growth, the feed channel would tend to narrow with a consequent increment of the effective cross-flow velocity (Fig. 5b, feed side). The shear stress thus thwarts the further deposition of foulants and promotes foulant back-transport, therefore preventing further growth of the

fouling layer [36-38]. During the late stage of filtration, the fouling layer thickness approached a near-stable value as the lift and drag forces reached equilibrium in the feed channel (see Fig 2a2). In parallel, also the flux approached a near-stable value (see Fig 2a1). Therefore, as overall effect, the mutual increase of both the average nominal driving force and of the overall resistance should lead to a self-compensation phenomenon during which the fouling thickness, the effective cross-flow velocity and the cake-enhanced temperature polarization reach near equilibrium and productivity reaches a near steady-state condition.

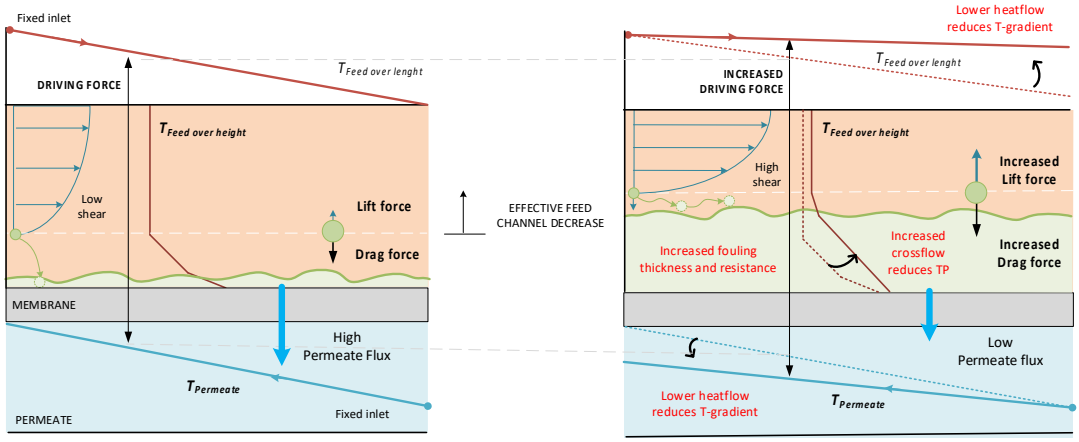

Fig. 5. Micro to macroscale analysis of the mechanisms occurring upon organic foulant deposition and fouling layer formation in direct contact membrane distillation, including influence on the hydrodynamic parameters, effects on temperature profiles and on the driving force. Left panel refers to conditions of clean membrane, right panel to conditions after cake layer formation. The experiment were performed with a feed solution consisting of 500 mg/L of humic acid and 20 mM of $CaCl_2$.

4 Conclusion

This study presented an analysis of organic fouling in membrane distillation under a wide range of temperature and cross-flow velocity conditions. During operation, the analysis of the fouling layer with OCT highlighted the linear correlation between layer thickness increase and flux reduction. An investigation of the main resistances to water vapor flux confirmed that the heat transfer was reduced due to fouling accumulation. In particular, the amount of heat

loss within the fouling layer grew at the expenses of lower heat loss due to convective heat (i.e., heat transported by water vapor flux) and to the two temperature polarizations at the feed and permeate side. Also, the average nominal driving force increased while the overall resistance also increased, overall reducing the water vapor flux. Results suggest that fouling resistance and the driving force evolved together and governed the fouling evolution dynamics over time. Fouling was found to be a dynamic phenomenon, whereby governing factors evolved together resulting in a final near steady-state productivity value as net result. This continuous process may be discretized in steps as follows:

(i) Fouling deposition increases the overall resistance to the water vapor flux.

(ii) The fouling layer and the related water flux decrement reduce the heat transferred from the feed to the permeate stream with the overall effect of an increase in average nominal driving force, i.e., bulk temperature difference between the feed and the permeate side.

(iii) As in the other membrane process, the driving force increase inevitably leads to an increment of the permeate drag force, which thereby promotes foulant transport and accumulation onto the membrane surface.

(iv) The mutual increments of the driving force and fouling resistance generate a self-compensation phenomenon which is responsible for the near-stable flux gradually approached during fouling development.

(v) The plateau is reached for both flux and fouling thickness as the gradual fouling accumulation also leads to an increase of the shear force in the feed channel that thwarts foulant deposition and counterbalances the increasing permeate drag force of foulant toward the membrane.

522 **Acknowledgements**

523 The research reported in this paper was supported by funding from King Abdullah University
524 of Science and Technology (KAUST), Saudi Arabia and by Politecnico di Torino, Italy.
525 Francesco Ricceri acknowledges funding from the CleanWaterCenter@PoliTo for his Ph.D.
526 scholarship (01_TRIN_CI_CWC).

Supplementary Material

Understanding organic fouling evolution in membrane distillation through driving force and resistance analysis

***Francesco Ricceri*[1,2],**

1: Department of Environment, Land and Infrastructure Engineering, Politecnico di Torino, Corso Duca degli Abruzzi, 24 – 10129 Torino (Italy)

2: CleanWaterCenter@PoliTo, Corso Duca degli Abruzzi, 24 – 10129 Torino (Italy), web: http://cleanwater.polito.it/

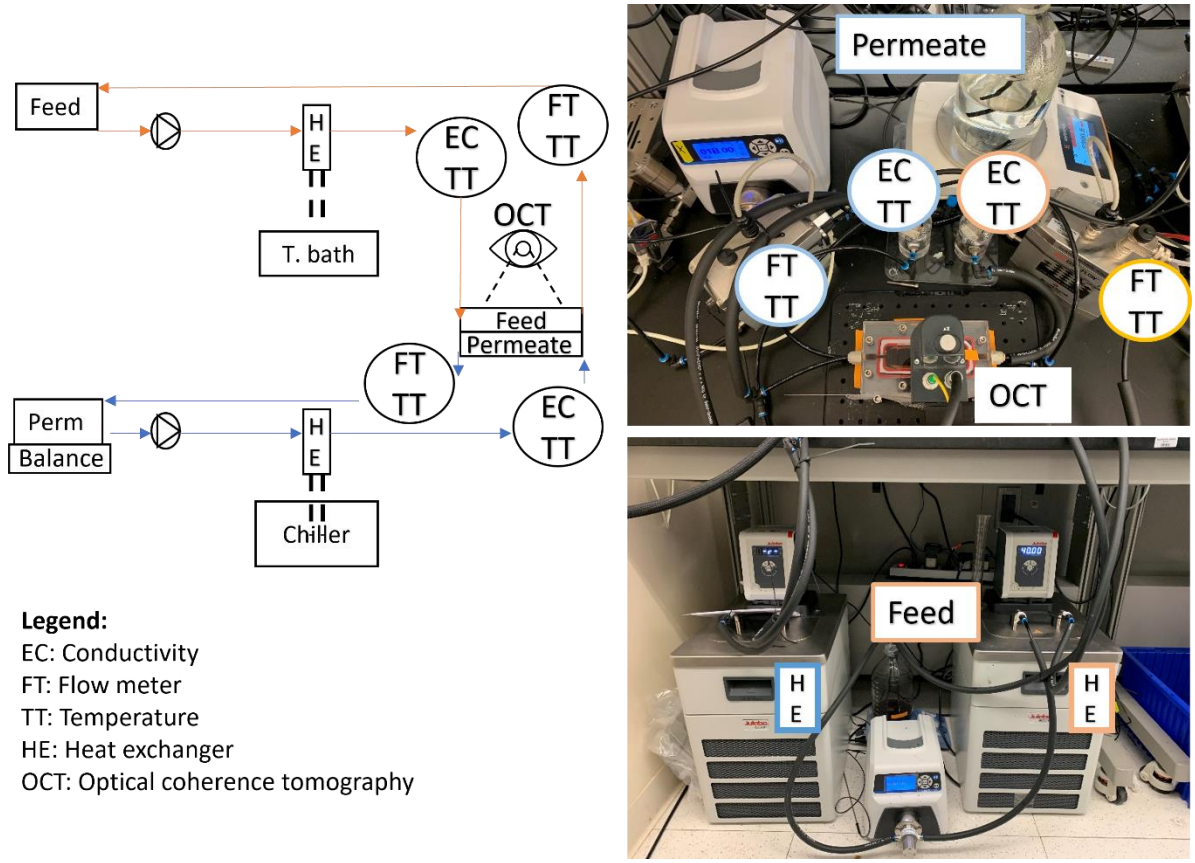

552

553 **Fig. S1.** Schematic representation and images of the setup used for this study. The orange
554 and blue lines are used for the warm feed and cold permeate respectively, the legend indicates
555 the acronymous used for each component. Regarding the OCT, only the camera positioned on
556 the transparent cell is shown in this picture.

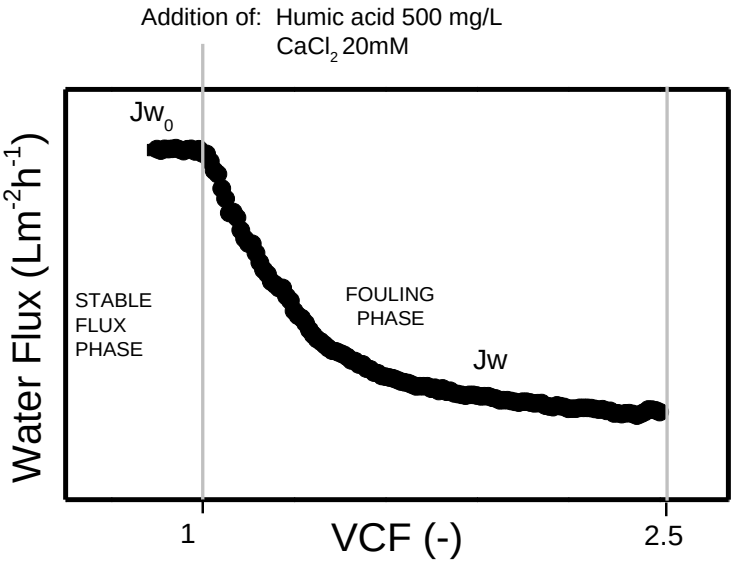

557

558 **Fig. S2.** Representative experimental determination of water flux through the MD membrane.
559 The protocol consisted of two stages: (i) the initial stabilization of flux, J_{w0}, using deionized
560 water, for roughly 30 min; (ii) the fouling phase started at the volume concentration (VCF)

equal to 1 and was carried out for a volume concentration factor of 2.5. Here, the flux is indicated by J_w.

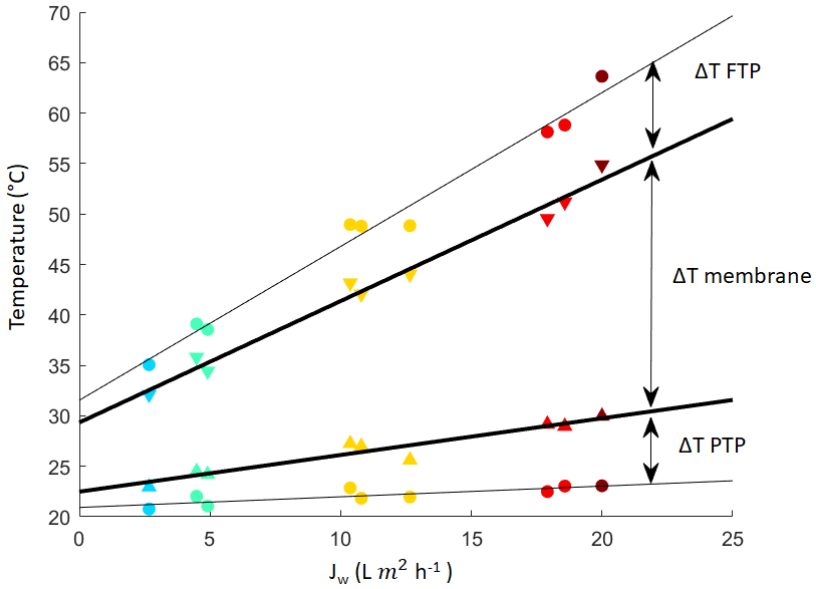

Fig. S3. Temperature profile between the feed and permeate bulk solutions before fouling (clean membrane). The profile was retrieved by implementing Eq. 3, related to the temperature profile in the presence of temperature polarization, for all the performed experiments (Table S1). The temperature drop across the membrane was retrieved as difference between the temperature values at the membrane interface. The fitting was performed to assess the temperature polarization and temperature difference across the membrane for any measured flux even during fouling.

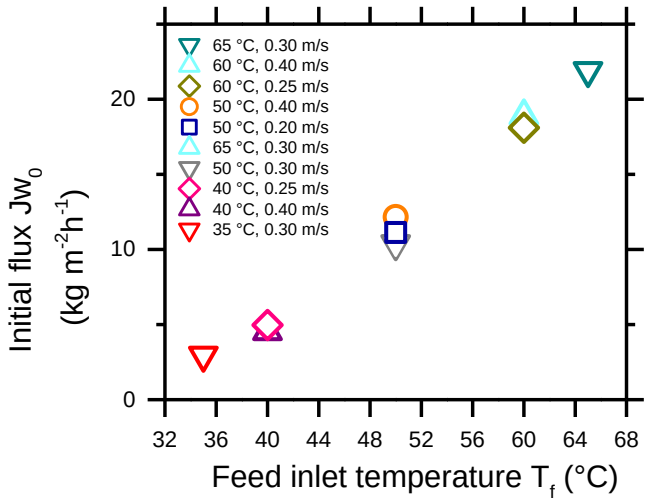

Fig. S4. Initial flux (Jw_0) as a function of the feed inlet temperature prior to foulant addition for the nine different tests reported in legend, each run with a different combination of temperature and cross-flow velocity. The list of experiment was designed by central composite

design method through Design Expert software, from a selected temperature range of 35-65 °C and a range of cross-flow velocity of 0.20-0.40 m/s.

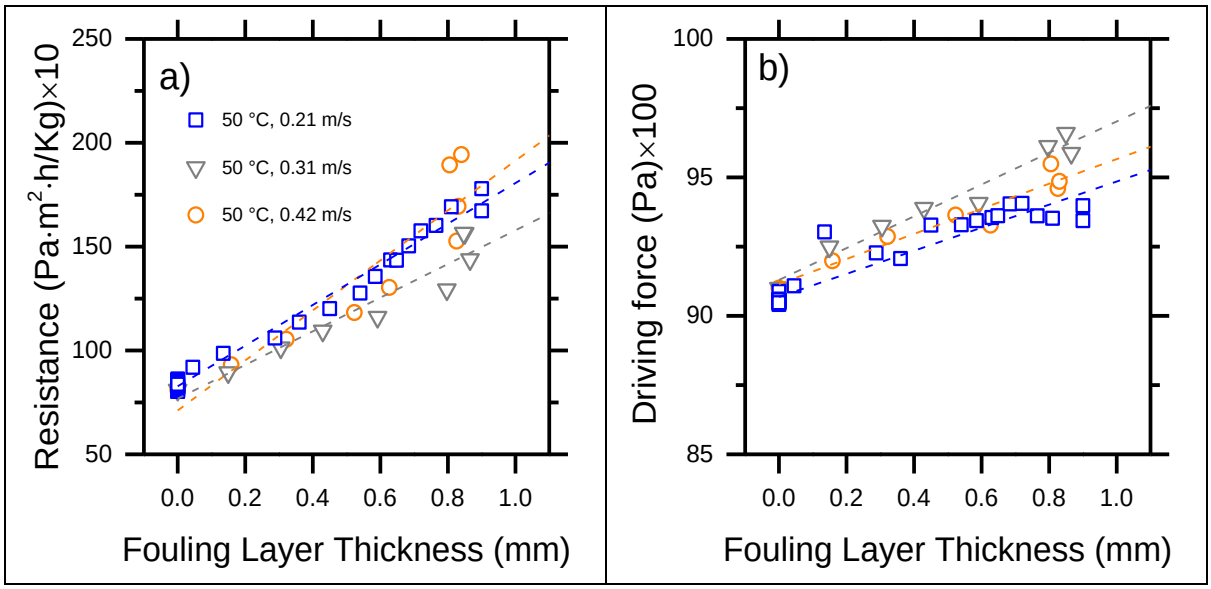

Fig. S5. Evolution of the (a) overall resistance and (b) average nominal driving force during fouling for the experiments performed at 50 °C. Results are included in Fig. 4 and are here reported by narrowing the y-axes range to better asses the increasing trends.

Table S1. List of experiments determined by a central composite design method in Design Expert software, a tool used to get efficient experimental protocols.

Experiment	
Feed temperature (°C)	Feed cross-flow velocity (m/s)
35	0.30
40	0.25
40	0.40
50	0.20
50	0.30
50	0.40
60	0.40
60	0.25
65	0.30

Table S2. Intercept, slopes and related standard error values of best lines fitting the average nominal driving force and foulant resistance when each is plotted against fouling thickness (dash lines showed in Fig. 4 of the main manuscript)

Experiment			Resistance (Pam2h/Kg)		Driving force (Pa)	
Feed Temperature (°C)	Cross-flow velocity (m/s)		Value	St.Error	Value	St.Error
35	0.30	Intercept	993.30	24.26	3211.02	14.3
		Slope	0.92	0.13	0.23	0.07
40	0.25	Intercept	852.61	35.50	4430.06	10.73
		Slope	1.14785	0.08	0.30	0.02
40	0.40	Intercept	881.13	46.97	4300.45	13.58
		Slope	0.97	0.19	0.27	0.05
50	0.20	Intercept	827.48	6.11	9068.42	9.53
		Slope	0.97	0.01	0.41	0.02
50	0.30	Intercept	768.28	55.62	9129.78	27.86
		Slope	0.81	0.08	0.57	0.04
50	0.40	Intercept	711.14	113.89	9114.81	31.03
		Slope	1.20	0.18	0.45	0.05
60	0.25	Intercept	961.08	26.19	16250.98	40.6
		Slope	1.27	0.04	0.58	0.06
60	0.40	Intercept	819.94	96.47	16121.9	27.25
		Slope	1.24	0.15	0.58	0.04
65	0.30	Intercept	784.43	97.04	20972.12	60.9
		Slope	1.53	0.13	0.48	0.08

References

[1] Y. Choi, G. Naidu, L.D. Nghiem, S. Lee, S. Vigneswaran, Membrane distillation crystallization for brine mining and zero liquid discharge: opportunities, challenges, and recent progress, Environmental Science: Water Research & Technology, 5 (2019) 1202-1221.

[2] B. Ashoor, S. Mansour, A. Giwa, V. Dufour, S. Hasan, Principles and applications of direct contact membrane distillation (DCMD): a comprehensive review, Desalination, 398 (2016) 222-246.

[3] E. Curcio, E. Drioli, Membrane distillation and related operations—a review, Separation and Purification Reviews, 34 (2005) 35-86.

[4] L.M. Camacho, L. Dumée, J. Zhang, J.-d. Li, M. Duke, J. Gomez, S. Gray, Advances in membrane distillation for water desalination and purification applications, Water, 5 (2013) 94-196.

[5] M. Gryta, M. Tomaszewska, K. Karakulski, Wastewater treatment by membrane distillation, Desalination, 198 (2006) 67-73.

[6] M.M. A Shirazi, A. Kargari, A review on applications of membrane distillation (MD) process for wastewater treatment, Journal of Membrane Science and Research, 1 (2015) 101-112.

[7] D. Hou, J. Wang, C. Zhao, B. Wang, Z. Luan, X. Sun, Fluoride removal from brackish groundwater by direct contact membrane distillation, Journal of Environmental Sciences, 22 (2010) 1860-1867.

[8] S. Srisurichan, R. Jiraratananon, A. Fane, Humic acid fouling in the membrane distillation process, Desalination, 174 (2005) 63-72.

[9] K.W. Lawson, D.R. Lloyd, Membrane distillation, Journal of membrane Science, 124 (1997) 1-25.

[10] L.N. Nthunya, M.F. Bopape, O.T. Mahlangu, B.B. Mamba, B. Van der Bruggen, C.A. Quist-Jensen, H. Richards, Fouling, performance and cost analysis of membrane-based water desalination technologies: A critical review, Journal of Environmental Management, 301 (2022) 113922.

[11] F. He, K.K. Sirkar, J. Gilron, Studies on scaling of membranes in desalination by direct contact membrane distillation: CaCO3 and mixed CaCO3/CaSO4 systems, Chemical Engineering Science, 64 (2009) 1844-1859.

[12] L.D. Tijing, Y.C. Woo, J.-S. Choi, S. Lee, S.-H. Kim, H.K. Shon, Fouling and its control in membrane distillation—A review, Journal of Membrane Science, 475 (2015) 215-244.

[13] L. Martínez-Díez, M.I. Vazquez-Gonzalez, Temperature and concentration polarization in membrane distillation of aqueous salt solutions, Journal of membrane science, 156 (1999) 265-273.

[14] P. Wang, M.M. Teoh, T.-S. Chung, Morphological architecture of dual-layer hollow fiber for membrane distillation with higher desalination performance, water research, 45 (2011) 5489-5500.

[15] E. Guillen-Burrieza, A. Ruiz-Aguirre, G. Zaragoza, H.A. Arafat, Membrane fouling and cleaning in long term plant-scale membrane distillation operations, Journal of membrane science, 468 (2014) 360-372.

[16] M. Gryta, M. Tomaszewska, J. Grzechulska, A. Morawski, Membrane distillation of NaCl solution containing natural organic matter, Journal of Membrane Science, 181 (2001) 279-287.

[17] F. Ricceri, M. Giagnorio, G. Farinelli, G. Blandini, M. Minella, D. Vione, A. Tiraferri, Desalination of produced water by membrane distillation: Effect of the feed components and of a pre-treatment by fenton oxidation, Scientific reports, 9 (2019) 1-12.

[18] J. Guo, L. Fortunato, B.J. Deka, S. Jeong, A.K. An, Elucidating the fouling mechanism in pharmaceutical wastewater treatment by membrane distillation, Desalination, 475 (2020) 114148.

[19] L. Fortunato, H. Elcik, B. Blankert, N. Ghaffour, J. Vrouwenvelder, Textile dye wastewater treatment by direct contact membrane distillation: Membrane performance and detailed fouling analysis, Journal of Membrane Science, 636 (2021) 119552.

[20] L. Fortunato, Y. Jang, J.-G. Lee, S. Jeong, S. Lee, T. Leiknes, N. Ghaffour, Fouling development in direct contact membrane distillation: Non-invasive monitoring and destructive analysis, Water research, 132 (2018) 34-41.

[21] F.A. Siddiqui, Q. She, A.G. Fane, R.W. Field, Exploring the differences between forward osmosis and reverse osmosis fouling, Journal of Membrane Science, 565 (2018) 241-253.

[22] F. Ricceri, M. Giagnorio, K.R. Zodrow, A. Tiraferri, Organic fouling in forward osmosis: Governing factors and a direct comparison with membrane filtration driven by hydraulic pressure, Journal of Membrane Science, 619 (2021) 118759.
[23] Q. She, R. Wang, A.G. Fane, C.Y. Tang, Membrane fouling in osmotically driven membrane processes: A review, Journal of Membrane Science, 499 (2016) 201-233.
[24] S. Srisurichan, R. Jiraratananon, A. Fane, Mass transfer mechanisms and transport resistances in direct contact membrane distillation process, Journal of membrane science, 277 (2006) 186-194.
[25] F. Ricceri, B. Blankert, N. Ghaffour, J.S. Vrouwenvelder, A. Tiraferri, L. Fortunato, Unraveling the role of feed temperature and cross-flow velocity on organic fouling in membrane distillation using response surface methodology, Desalination, 540 (2022) 115971.
[26] L. Mariah, C.A. Buckley, C.J. Brouckaert, E. Curcio, E. Drioli, D. Jaganyi, D. Ramjugernath, Membrane distillation of concentrated brines—Role of water activities in the evaluation of driving force, Journal of Membrane Science, 280 (2006) 937-947.
[27] A.S. Alsaadi, A. Alpatova, J.-G. Lee, L. Francis, N. Ghaffour, Flashed-feed VMD configuration as a novel method for eliminating temperature polarization effect and enhancing water vapor flux, Journal of Membrane Science, 563 (2018) 175-182.
[28] A. Hausmann, P. Sanciolo, T. Vasiljevic, U. Kulozik, M. Duke, Performance assessment of membrane distillation for skim milk and whey processing, Journal of dairy science, 97 (2014) 56-71.
[29] M. Laqbaqbi, J.A. Sanmartino, M. Khayet, C. García-Payo, M. Chaouch, Fouling in membrane distillation, osmotic distillation and osmotic membrane distillation, Applied Sciences, 7 (2017) 334.
[30] R.W. Field, G.K. Pearce, Critical, sustainable and threshold fluxes for membrane filtration with water industry applications, Advances in colloid and interface science, 164 (2011) 38-44.
[31] T.-T. Nguyen, C. Lee, R.W. Field, I.S. Kim, Insight into organic fouling behavior in polyamide thin-film composite forward osmosis membrane: Critical flux and its impact on the economics of water reclamation, Journal of Membrane Science, 606 (2020) 118118.
[32] X.-y. Li, X.-m. Wang, Modelling of membrane fouling in a submerged membrane bioreactor, Journal of Membrane Science, 278 (2006) 151-161.
[33] L. Fortunato, M. Li, T. Cheng, Z.U. Rehman, W. Heidrich, T. Leiknes, Cake layer characterization in activated sludge membrane bioreactors: real-time analysis, Journal of membrane science, 578 (2019) 163-171.
[34] Z. Ding, L. Liu, Z. Liu, R. Ma, Fouling resistance in concentrating TCM extract by direct contact membrane distillation, Journal of Membrane Science, 362 (2010) 317-325.
[35] A. Alkhatib, M.A. Ayari, A.H. Hawari, Fouling mitigation strategies for different foulants in membrane distillation, Chemical Engineering and Processing-Process Intensification, 167 (2021) 108517.
[36] S. Goh, Q. Zhang, J. Zhang, D. McDougald, W.B. Krantz, Y. Liu, A.G. Fane, Impact of a biofouling layer on the vapor pressure driving force and performance of a membrane distillation process, Journal of Membrane Science, 438 (2013) 140-152.
[37] R.W. Field, J.J. Wu, On boundary layers and the attenuation of driving forces in forward osmosis and other membrane processes, Desalination, 429 (2018) 167-174.
[38] R. Schofield, A. Fane, C. Fell, Gas and vapour transport through microporous membranes. II. Membrane distillation, Journal of Membrane Science, 53 (1990) 173-185.